Astron. Astrophys. 262, 624–633 (1992)

ASTRONOMY
AND
ASTROPHYSICS

The IRAM interferometer on Plateau de Bure

S. Guilloteau, J. Delannoy, D. Downes, A. Greve, M. Guélin, R. Lucas, D. Morris, S. J. E. Radford, J. Wink, J. Cernicharo, T. Forveille, S. Garcia-Burillo, R. Neri, J. Blondel, A. Perrigouard, D. Plathner, and M. Torres

Institut de Radioastronomie Millimétrique (IRAM), F-38406 Saint Martin d'Hères, France

Received January 13, accepted April 4, 1992

Abstract. The IRAM interferometer on Plateau de Bure has three 15 m diameter antennas presently equipped with low noise receivers for the 80-115 GHz band. Baselines extend 160 m north-south and 288 m east-west. There are two digital cross-correlators, a wide band continuum correlator and a narrow band spectral correlator. The instrument's high sensitivity is a result of its relatively large antennas.

Key words: instrumentation: interferometers – telescopes – radio lines: molecular: circumstellar – radio lines: molecular: interstellar

1. Introduction

Two historical trends in radio astronomy, towards ever higher frequencies and ever finer spatial resolution, are evident in the current generation of millimeter wave interferometers. These instruments provide images with a resolution of a few arcseconds of dust and molecular gas in outflows from protostars, circumstellar envelopes around evolved stars, and dense cores of molecular clouds in our Galaxy, and of the distribution of molecular gas in other galaxies. Since all of these objects are cool, typically 10–500 K, observations are limited by sensitivity; signal-to-noise ratios larger than about one hundred are exceptional. Here we describe the IRAM interferometer, whose high sensitivity is a result of its relatively large antennas.

2. The instrument

The IRAM interferometer on Plateau de Bure (Figs. 1 & 2) consists of three 15 m diameter antennas. These can be placed on 26 stations arrayed along a T shaped rail track that extends 160 m north-south and 288 m east-west. It is presently equipped with low noise receivers for the 80-115 GHz band. Two digital cross-correlators, a wide band continuum correlator and a narrow band spectral correlator, measure the complex visibility amplitudes, which are then recorded by the control computer.

Design work started in 1979. After completion of the cable car that provides the only access to the Plateau de Bure, construction began in 1983 and by the fall of 1985 the tracks were complete. The first antenna was assembled by October, 1986, and single dish test observations began the following June. In December, 1988, the first fringes were obtained with two antennas and interferometry with all three antennas was first done in June, 1989. The interferometer was dedicated in September, 1989, and the first proposals from guest investigators were received in October, 1990.

Send offprint requests to: S. Guilloteau

2.1. Site

Plateau de Bure, about 100 km south of Grenoble near St. Etienne-en-Dévoluy in the Département des Hautes Alpes, France, was selected as the interferometer site because of its altitude and flatness. The Plateau has more than 2 km^2 of relatively flat ground above 2500 m altitude, which is probably unique in Europe, and baselines as long as 1.5 km can be constructed. The array phase center is 5°54′28.5″ E longitude and 44°38′2.0″ N latitude and at the antennas' Cassegrain foci, 8 m above the tracks, the altitude is 2560 m. There is no road to the Plateau so all personel and material are transported to the site by *téléphérique*. In addition to the interferometer itself, the observatory complex includes a hangar large enough to house three antennas at once, living quarters, offices, laboratories, workshops, and the interferometer control room. Ambient temperatures range from −25° C to +25° C and the precipitable water vapor, determined both during site tests (Greve 1978) and from mm wave atmospheric transmission measurements, is often less than 2 mm, particularly in winter.

2.2. Antennas

The three antennas (Delannoy 1985) are mounted on fully steerable azimuth-elevation fork mounts that incorporate self propelled transporters for moving the antennas along the rail tracks between stations. Each is a Cassegrain telescope (Table 1) with the focus 302 mm from the intersection of the mount's azimuth and elevation axes, which were aligned to ±0.2 mm. An additional telescope fabricated in the same series became the SEST (Booth et al. 1989) installed on a fixed pedestal on La Silla, Chile.

Each primary mirror is composed of 176 panels, 60 mm thick and typically 1 m^2 in area, arranged in six concentric rings around a 1.45 m central aperture. The panels and secondary mirrors are sandwiches of aluminum honeycomb cores between carbon fiber skins with a 40 nm thick aluminum reflecting surface protected by a 30 μm film of Hostaflon (polymerized CF_2Cl_2). Although the aluminum layer is very thin, the impedence mismatch at this surface is so large that more than 99% of the incident radiation is reflected (Delannoy 1991). Because of this shiny mirror surface, however, the antennas must not be pointed within 35° of the Sun. To keep the reflecting surface ice free during bad weather, it

Fig. 1. The three antennas of the IRAM interferometer. (Photo by D. Downes.)

Fig. 2. View toward NW of the IRAM observatory on Plateau de Bure . The three antennas are stationed on the north track and the living quarters and assembly hangar are seen to the left of the white cable car station. The small dome houses a 2.5 m diameter millimeter wave telescope (Castets et al. 1988). (Photo by D. Robert.)

Table 1. Telescope characteristics

Optics	Cassegrain
Primary mirror	parabolic
diameter	15 m
focal ratio	0.325
Secondary mirror	hyperbolic
diameter	1.55 m
magnification	15.7
Cassegrain to prime focus	7.834 m
Geometric blockage	3.5%
Receiver illumination edge taper	14 dB
Beam size (90 GHz)	55″
Primary mirror error budget	(r. m. s.)
Panels	
surface accuracy	15 μm
wind (14 m s^{-1}) and gravity	4 μm
thermal deformations	15 μm
Backstructure	
maximum wind (14 m s^{-1})	37 μm
gravity (after homology)	11 μm
thermal deformations	10 μm
Total (r. m. s.)	45 μm
Holography measurements	(r. m. s.)
overall surface	73 μm
amplitude weighted aperture	61 μm
Efficiencies at 90 GHz (see text)	
ϵ_{ap}	65%
ϵ_{for}	93%
ϵ_{mb}	80%

can be heated electrically. The panels are attached by motorized adjustment screws to a lightweight, homologous, carbon fiber and steel backstructure mounted on a rigid central hub. The subreflector is supported from the backstructure by four carbon fiber legs.

Since thermal gradients in the telescope structure and mount adversely affect pointing accuracy and telescope efficiency, considerable attention was paid to the thermal design (Delannoy 1985; Greve et al. 1992). Carbon fiber was used extensively because of its stiffness, lightness, and low coefficient of thermal expansion. The fork mount is covered with polyurethane foam insulation and clad with a double walled aluminum radiation shield. The rear of the mirror backstructure is also clad with aluminum panels. This passive insulation is sufficient to reduce temperature differences between the fork arms to $< 2°$ C and deformations of the mirror surface to $< 18\,\mu$m under all conditions.

Homologous deformations of the telescope structure and mount imperfections are compensated with a trigonometric pointing model. Parameters for this model were initially measured by observing stars with optical telescopes mounted off-axis in the receiver cabins and later verified by observing radio continuum sources. Since most of the model parameters are telescope constants, however, and the station inclination is measured with an inclinometer, only the azimuth encoder zero must in principle be redetermined when an antenna is moved. The nominal pointing accuracy, $< 4''$ r. m. s., is regularly achieved during radio pointing sessions that accompany each array reconfiguration.

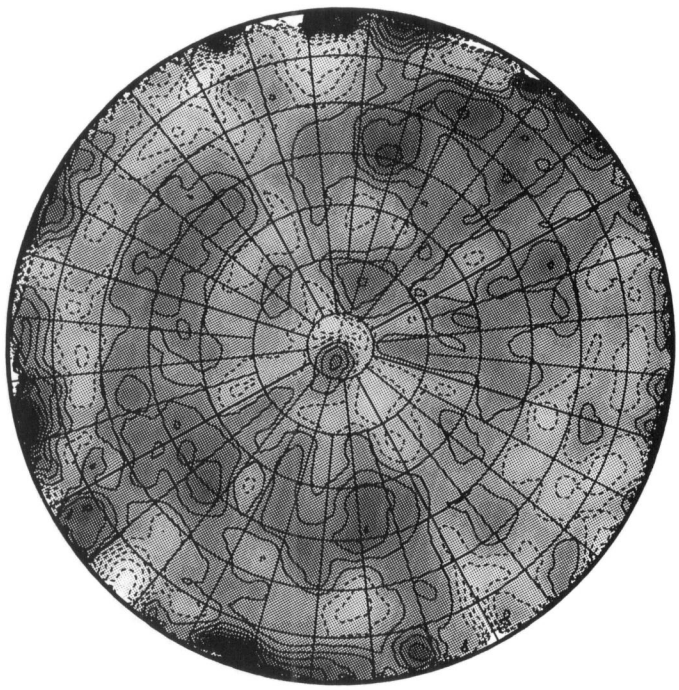

Fig. 3. Holographic image at 86 GHz of one antenna after the initial setting of the panels with a theodolite and tape. In this front view of the primary mirror, dashed contours represent displacements toward the secondary mirror and the contour interval is 50 μm.

Individual mirror panels have an average r. m. s. surface accuracy better than 15 μm. After assembly the mirror surfaces were adjusted with a theodolite and steel tape. Subsequent holography measurements (Fig. 3) have confirmed the overall surface accuracy is 75 μm r. m. s., or 60 μm r. m. s. when weighted by the receiver illumination pattern, and promise improvement of the surfaces to 45 μm r. m. s. At 90 GHz the antennas presently have a forward efficiency $\epsilon_{for} = 93\%$, a main beam efficiency $\epsilon_{mb} = 80\%$, an aperture efficiency $\epsilon_{ap} = 65\%$, and a point source sensitivity $\gamma = S/T_a^* = 2k\,\epsilon_{for}/\epsilon_{ap}\,A = 22\,\mathrm{Jy\,K^{-1}}$, where A is the geometric area, S is the source flux density, and T_a^* is the antenna temperature corrected for atmospheric, rear spillover and scattering, and resistive losses (see Downes 1989).

2.3. Array

Along the three rail tracks are 26 stations spaced at multiples of 8 m: a central station at the intersection of the tracks, eleven stations along the 160 m north track, six along the 96 m west track, and eight along the 192 m east track (Fig. 4). The north arm is oriented 2°31′ W of N and the east-west track 12°29′ S of E, so the two arms cross at 75°. A spur track runs parallel to the east-west track from station N13 to the assembly hall. In addition to electrical power and signal connections, each station is equipped with two alignment sockets and eight footpads to which an antenna is clamped during observations. The altitudes of the stations are identical to within 1 mm and the maximum inclination of any station from the astronomical vertical is 50″, with typical values around 20″.

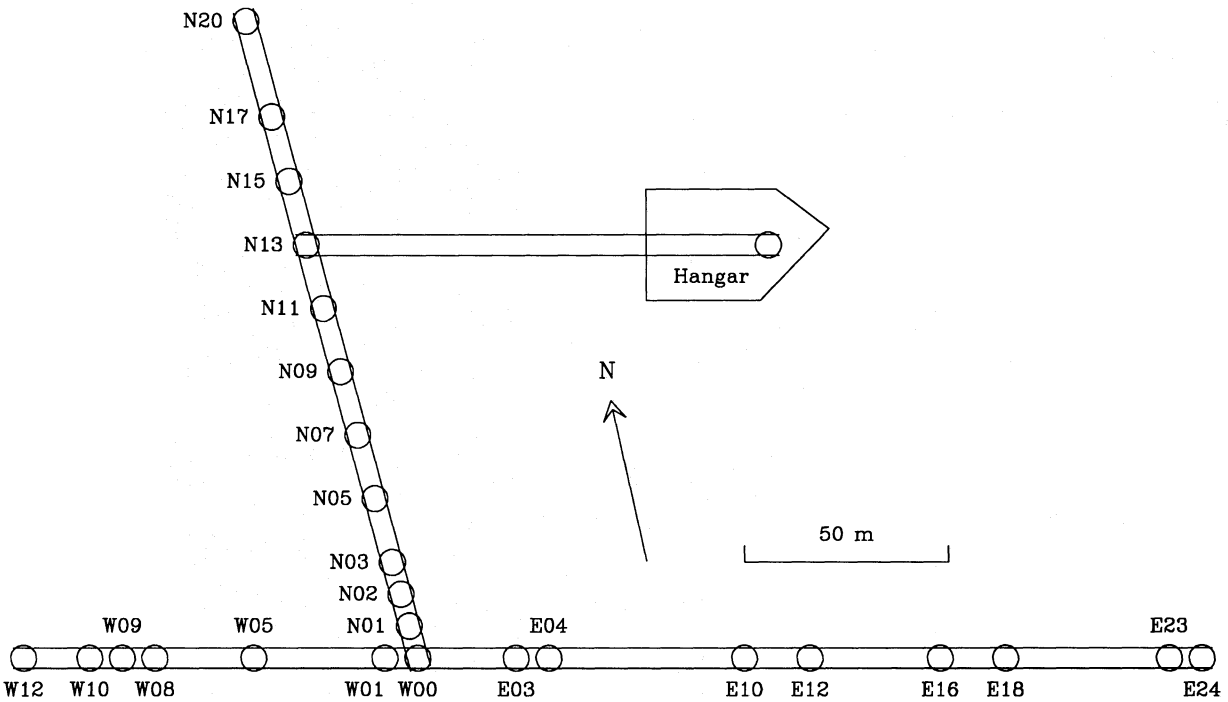

Fig. 4. Track and station layout of the IRAM interferometer on Plateau de Bure. Station names are in units of 8 m from the intersection (station W00), i.e., station N05 is 40 m from the intersection along the north track.

2.4. Receivers

For initial operation, the IRAM interferometer is equipped with receivers tunable from 80–115 GHz. Two of the receivers have niobium junction SIS mixers (Lehnert et al. 1991) cooled to 3 K while the third receiver has a Schottky mixer cooled to 15 K. The SIS junctions and all three receivers were made in the IRAM receiver laboratory. Phase locked Gunn diode oscillators generate the local oscillator (LO_1) signals, which are injected into the corrugated scalar feed horns through a quasi-optic diplexer. The illumination taper at the edge of the primary mirror is 12 dB. At the first intermediate frequency, $IF_1 = 1.5$ GHz, is a chain of cooled HEMT amplifiers. For calibration an ambient temperature absorber is slid in front of the horn and during single dish observations a rotating chopper wheel switches the beam 130″ in elevation at 16 Hz. The receivers have instantaneous bandwidths of 600 MHz and are normally operated in DSB mode, although the SIS receivers can be tuned to reject the USB by 3–6 dB. DSB receiver temperatures at 90 GHz are 40 and 70 K for the SIS receivers (Fig. 5) and 120 K for the Schottky receiver. Typical SSB system temperatures, including atmospheric losses, are 250-400 K (T_a^*).

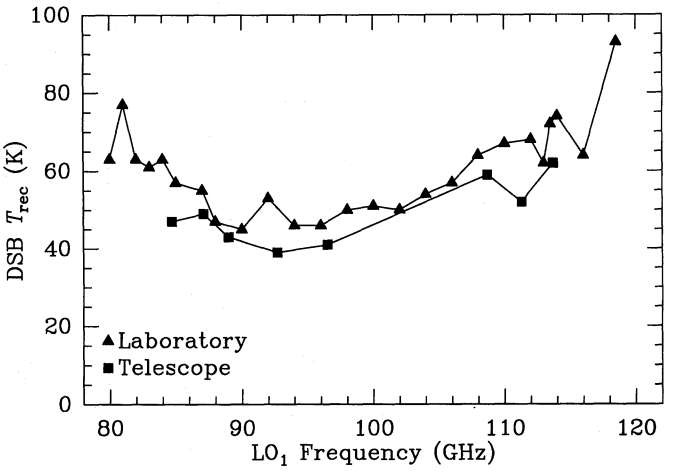

Fig. 5. Measured DSB noise temperature of a niobium junction SIS mixer receiver installed on the IRAM interferometer. Triangles show laboratory measurements and squares show measurements at the telescope.

2.5. Frequency synthesis and signal transmission

The frequency synthesis and signal transmission system generates phase synchronous oscillator signals, transmits them to the antennas, and transports the receiver outputs from the antennas back to the correlator room (Fig. 6).

Three frequency down conversions are used. In each receiver the sky frequency (RF) and LO_1 signals are mixed to generate a 1.5 GHz IF_1. This signal is then amplified, filtered, and equalized before it is down converted to the 100-600 MHz IF_2 band by an LSB mixer with an LO_2 near 1875 MHz. The IF_2 signal is then transmitted to the correlator room where it is divided into ten adjacent 50 MHz wide IF_3 basebands by five image rejection mixers with sideband separations of 25 dB. The correlators then sample the IF_3 basebands.

All frequencies are derived from a 5 MHz master oscillator locked to a low drift (< 1 ms week^{-1}) quartz clock synchronized weekly with LF time signals broadcast by the Neuchâtel Observatory (Switzerland). This 5 MHz pilot is used to generate a $\delta = 500$ kHz signal for the cable phase measurement (see below), an $\varepsilon = 100$ MHz phase rotation signal for LO_1, and the 150, 250, 350, 450, and 550 MHz LO_3 signals used by the image rejection

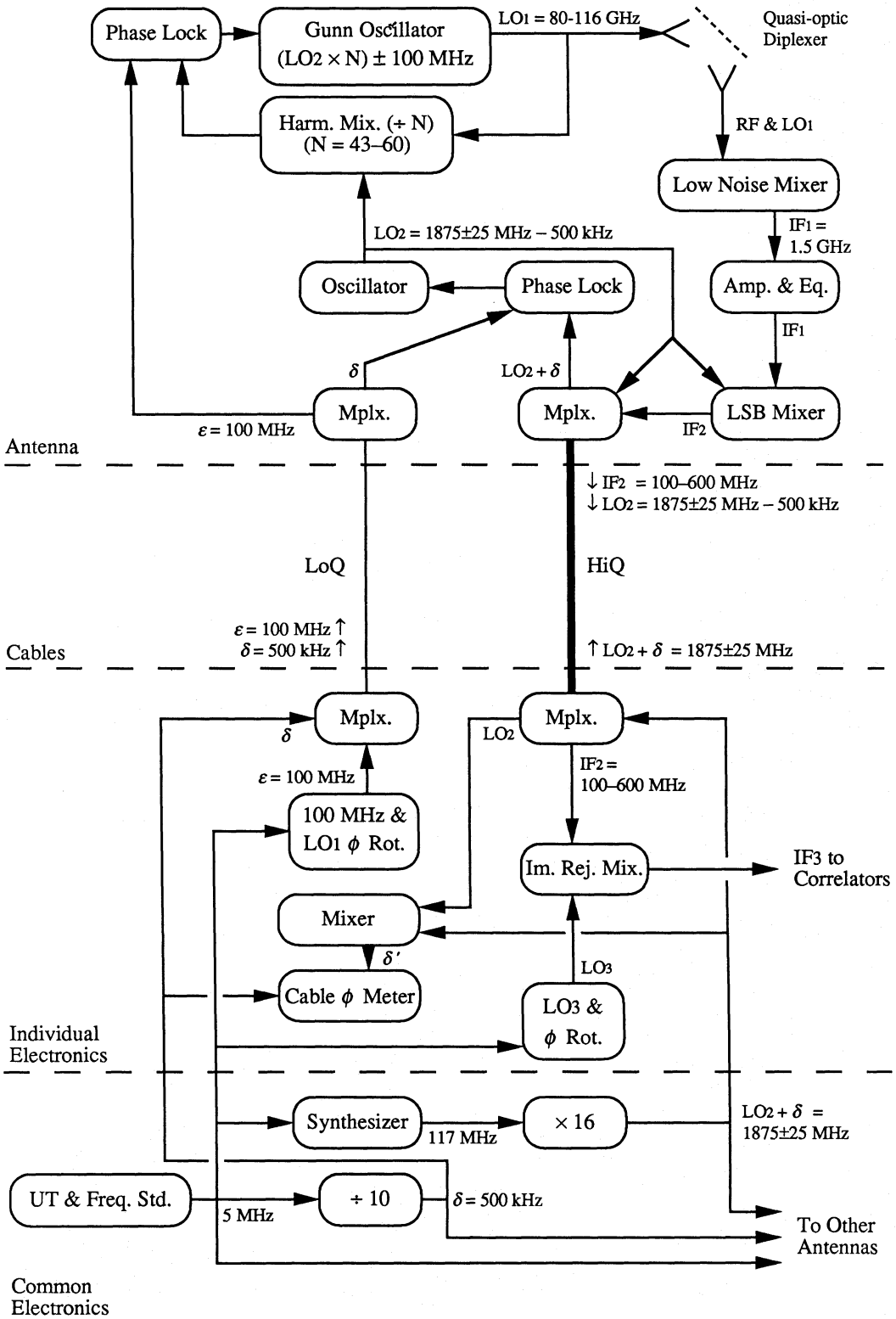

Fig. 6. Block diagram of frequency synthesis and signal transmission system. Except for the UT clock, the 5 MHz frequency standard, and the frequency synthesizer and multiplier, all elements are duplicated for each antenna.

mixers to divide the IF_2 band.

The master oscillator also drives a programmable frequency synthesizer whose output, $\nu_{syn} = 117 \pm 1.5$ MHz, is multiplied by sixteen to generate an 1875 ± 25 MHz reference signal, $LO_2 + \delta = 16\nu_{syn}$. At each antenna this reference signal and δ drive a phase locked oscillator that produces the LO_2 signal used for the second down conversion $IF_2 = LO_2 - IF_1$. The Gunn diode oscillator that generates LO_1 is phase locked to an harmonic of LO_2 offset by $\pm\varepsilon$.

Since both LO_1 and LO_2 are generated from one synthesizer, IF_1 is variable by up to 50 MHz. For example, if the LO_1 phase locked loop is closed so that $LO_1 = NLO_2 + \varepsilon$, then the signal frequency ν_s corresponding to a given point in the IF_2 band will be

$$\nu_s = [(N \pm 1)LO_2 \mp IF_2 + \varepsilon]/(1 - v/c), \quad (1)$$

where v is the Doppler correction velocity and the upper signs are used if the signal is in the upper receiver sideband. These signs are reversed for the image frequency, ν_i, so the difference, $\nu_s - \nu_i = 2\,IF_1 = \pm 2(LO_2 - IF_2)/(1 - v/c)$, depends on the Doppler correction. Consequently, the Doppler tracking is exact only for one sideband. This effect is only noticeable, however, with high spectral resolution, < 312 kHz channel^{-1}.

Pairs of underground coaxial cables connect each antenna to the electronics room. Separate cables are used for each station, but to simplify the equalization circuits all the cables have the same physical length, ≈ 250 m. A high quality (HiQ) cable transports the $LO_2 + \delta$ reference signal from the master oscillator to the antenna and brings the IF_2 and LO_2 signals back to the correlator room. The two lower frequency signals, δ and ε, are sent to the antennas on a lower quality cable (LoQ).

The electrical lengths of the HiQ cables are measured continuously. At each antenna, the $LO_2 + \delta$ reference signal received from the central electronics is mixed with the $\delta = 500$ kHz signal and sent back down the same cable. In the correlator room, this returned signal, LO2, is mixed with the reference signal and the phase difference in the 500 kHz carrier is measured. The resulting phase correction is applied to LO_1 through ε.

All delays are generated digitally in the correlators. Fringes are stopped by rotating the local oscillator phases. To stop the fringes for every IF_3 baseband and for both receiver sidebands, phase rotators for both LO_1 and LO_3 are necessary. The LO_1 phases are also switched by $n\pi/2$ with 128 state, 4 s period Walsh functions to separate the receiver sidebands and reduce cross-talk between the antennas. Demodulation occurs synchronously in the correlators, and the measured sideband separation is better than 30 dB.

2.6. Correlators

Two digital complex cross-correlators are available: a wide band, *continuum* correlator and a narrow band, *spectral* correlator. These are always used simultaneously, so continuum flux measurement is a by-product of any spectral line project. To calibrate their frequency dependent phase and amplitude responses, the correlators can be connected to a common noise source instead of the IF signals from the antennas. Besides the correlators there are three other backends: a multichannel continuum detector for amplitude and atmospheric opacity calibration and, for single dish observations, a 128×100 kHz filter bank and a high precision continuum detector.

The continuum correlator has ten adjacent 50 MHz wide channels for each baseline, one for each of the IF_3 basebands. By sampling each baseband at 100 MHz with 15 levels and keeping 4 bits (16 levels) of the cross products, this correlator achieves high (97%) efficiency (Heintz & Emerson 1985). No gain control is needed because the fine quantization steps give a ± 2 dB dynamic range. Both real and imaginary parts of the cross correlation amplitudes are measured simultaneously; for the imaginary part the signal phase is digitally shifted by $\pi/2$ after sampling and before multiplication. Because of the large channel width, small delay steps are required to match the coherence loss to the high digital sensitivity. Delay steps smaller than the sampling rate (from 10 ns down to 0.25 ns) are introduced by shifting the sampler clocks.

The reconfigurable spectral correlator provides four subbands of 32 channels each with channel spacings from 39 kHz to 1.25 MHz. Because the subbands cannot be tuned arbitrarily in the IF_2 band, but must sample the fixed frequency IF_3 bands, the maximum contiguous bandwidth is 80 MHz, although two bands of 80 MHz can be selected with a 20 MHz gap between them. This correlator (Urry et al. 1985) uses three level sampling so it has an efficiency of 81% and an adjustable input gain control gives it a $+6$ to -12 dB dynamic range. Because of channel shape and apodization the effective resolution is about 1.6 times broader than the nominal channel spacing and the noise bandwidth is 1.87 times the channel spacing.

2.7. Control system

The IRAM interferometer is controlled by a central Digital VAX 3400 computer linked to several embedded microprocessors through a CAMAC interface. Observations are coordinated and sequenced by the user interface program, which runs predefined procedures for long or repetitive observations. A second VAX, which shares disk space with the control computer, is used for almost real-time and off-line data reduction.

Each antenna has a microprocessor that controls the azimuth and elevation drive servo loops, movements of the antenna transporter, and several safety interlocks, including one that prevents pointing an antenna too close to the Sun. The subreflector position is controlled directly by the control computer. Receivers are tuned through the control computer and the CAMAC interface either manually or by an automatic tuning program. The continuum correlator has its own microprocessor to demodulate the LO_1 phase switching and to integrate the outputs over 4 s periods, while the spectral correlator is directly controlled by the central computer. The multichannel continuum detector, filter bank, and high precision continuum detector have microprocessors that synchronize data acquisition with the beam switch.

The basic data acquisition interval is 4 s, the period of the Walsh function phase switching cycle. During this interval the control computer does the necessary astrometric calculations and supplies the antenna microprocessors with pointing and tracking information every 125 ms. The LO_1 and LO_3 phases, their rates, and the delays are updated every 4 s to follow the changing geometrical path and fringe rate. At the end of each 4 s interval, the data are read from the correlator output registers, formatted, and stored on disk. The LO_1 frequency is updated every 10 min to compensate for the Doppler effect.

The user interface program, OBS (Guilloteau 1990), is similar to the one used at the IRAM 30 m telescope. It is based on a command interpreter that allows flexible programming with

parametrized observing procedures. There are commands for instrument setup, IF bandpass and atmospheric transmission calibration, and receiver gain ratio, delay offset, pointing, and focus measurements. Standard procedures are used for most observations, including pointing sessions, baseline determination, image synthesis, and even series of snapshots. In addition to the high level interface, individual parts of the system can be controlled independently from a menu. An alarm notifies the array operator of any anomalies, including the end of an observing procedure.

2.8. Data reduction

Routine calibrations are automatically applied to the raw data by the off-line computer in almost real-time and the data are then compressed by averaging the basic 4 s integrations over typically one minute. These partially calibrated, compressed data can be monitored with an immediate display of amplitudes and phases. Both raw and compressed data are archived daily on magnetic tapes. The compressed data is later distributed to guest investigators for further analysis.

A dedicated program, CLIC (Lucas 1991), was developed for reducing interferometer data. Its basic facilities include data display, editing, and compression, and such routine calibration steps as correlator clipping corrections, Fourier transformation of spectral correlator data from the time to the frequency domain, IF bandpass calibration, and amplitude and atmospheric opacity calibration. Observations of reference sources are used to calibrate the RF bandpass, the flux scale, and the source amplitude and phase. Calibrated visibilities are then tabulated for further processing. There are also several specialized routines for interferometer setup, including reduction of interferometric pointing and focus measurements, and determination of the interferometer baseline lengths from observations of point sources with known positions.

Maps can be processed interactively with the GILDAS (Guilloteau & Forveille 1989) image processing system. Available tasks include direct measurement of source positions and sizes from *uv* plane visibility data, map construction from *uv* data, and CLEANing maps with any of several variants of the basic algorithm. Mosaic construction and deconvolution is also possible with a modified CLEAN program, and single dish data can be merged with interferometer data to provide short spacing information. Data also can be translated into UVFITS or FITS formats for transport to other image processing software.

Table 2. Standard configuration sets

Config.	Stations	BC	CD
B1	N20–W05–E18	•	
B2	N20–W12–E24	•	
B3	N17–W08–E24	•	
C1	N13–N05–W12	•	•
C2	N03–W08–W05	•	•
C3	N13–W00–E18	•	•
D1	N20–W12–E10		•
D2	N17–N07–N01		•
D3	N01–N05–W05		⋆

⋆ Optional configuration

2.9. Operation

The interferometer is operated as a full service instrument by the IRAM staff. The array is reconfigured roughly every three weeks and six to ten projects are observed in parallel. Moving all three antennas requires five to eight hours and a comparable time is needed for the subsequent pointing, delay, and baseline measurements. Baselines are determined to ± 0.3 mm from observations of strong continuum point sources.

3. Performance and capabilities

Because of its large dishes the IRAM interferometer has high sensitivity so it is especially suited for high resolution studies of weak sources. The high sensitivity also improves the calibration accuracy since point sources as weak as 0.5 Jy can be used as phase calibrators. Since more sources can be used, they can be chosen closer to the program objects. Phase errors introduced by baseline errors or atmospheric inhomogeneities are thereby reduced and the dynamic range and absolute positioning of the map improved. The built-in calibration noise source also helps in obtaining high spectral dynamic range.

3.1. Angular resolution

Two standard sets of configurations, named BC and CD (Table 2), are reasonably well suited for observations at all declinations. Set BC gives an angular resolution $\approx 2''$ at 90 GHz, but requires six observing configurations (18 baselines) and the synthesized beam is significantly elongated at low declinations. Set CD, on the other hand, gives lower resolution, $\approx 3.5''$ at 90 GHz, but it uses only five configurations (15 baselines) and the beam is approximately circular at all positive declinations. An optional, very compact configuration can also be used for sensitivity limited or mosaic observations. Table 3 summarizes the beam sizes with natural weighting for observations at 90 GHz limited to 6 h before and after source transit and elevations above 15°.

The field of view is limited by the antenna beam, whose FWHM is $55''$ at 90 GHz. It is possible to image a wider field of view by mosaicing. The shortest possible spacing is 24 m so even though projection shortens the effective baselines, structures larger than about $30''$ are heavily resolved.

3.2. Sensitivity

The r.m.s. uncertainty in a measurement of the flux of a point source with an array of N antennas and bandwidth $\Delta\nu$ is (Thompson et al. 1989)

$$\delta S = \frac{\gamma\, T_{\rm sys}}{\eta_{\rm c}\eta_{\rm p}\eta_{\rm j}\sqrt{N(N-1)}\sqrt{\Delta\nu\,\tau}}, \qquad (2)$$

where τ is the integration time, $T_{\rm sys}$ is the system temperature corrected for atmospheric losses, γ is point source sensitivity of the individual antennas (§2.2), $\eta_{\rm c}$ is the correlator efficiency, and the instrumental decorrelation, $\eta_{\rm j}$, and atmospheric decorrelation, $\eta_{\rm p}$, are related to the oscillator phase jitter, $\sigma_{\rm j}$, and atmospheric phase noise, $\sigma_{\rm p}$, by $\eta_{\rm j}\eta_{\rm p} = \exp[-(\sigma_{\rm j}^2 + \sigma_{\rm p}^2)/2]$.

For the IRAM interferometer $N = 3$ and at 90 GHz, $\gamma = 22\,{\rm Jy\,K^{-1}}$ and $T_{\rm sys} = 300$ K SSB typically. For the spectral correlator $\eta_{\rm c} = 81\%$ and $\Delta\nu$ is the noise equivalent bandwidth, 1.87 times the channel separation, while for the continuum correlator $\eta_{\rm c} = 97\%$ and DSB measurements have $\Delta\nu = 1$ GHz. The oscillator jitter $\sigma_{\rm j} \approx 25°$ at 90 GHz and increases linearly with

Table 3. Synthesized beam sizes at 90 GHz

Dec.	Configuration Set BC				Configuration Set CD			
	major axis (FWHM)	minor axis (FWHM)	angle (a)	sidelobe level	major axis (FWHM)	minor axis (FWHM)	angle (a)	sidelobe level
+80°	2.3″	2.2″	80°	5%	4.1″	3.8″	70°	5%
+60°	2.3″	2.1″	65°	10%	4.1″	3.5″	85°	5%
+40°	2.4″	2.1″	45°	15%	4.2″	3.5″	85°	10%
+20°	2.9″	2.1″	30°	20%	4.3″	3.8″	85°	15%
0°	3.6″	2.1″	25°	45%	4.7″	4.2″	15°	35%
−20°	5.3″	1.9″	12°	30%	7.1″	4.0″	0°	20%

(a) Position angle of major axis E from N

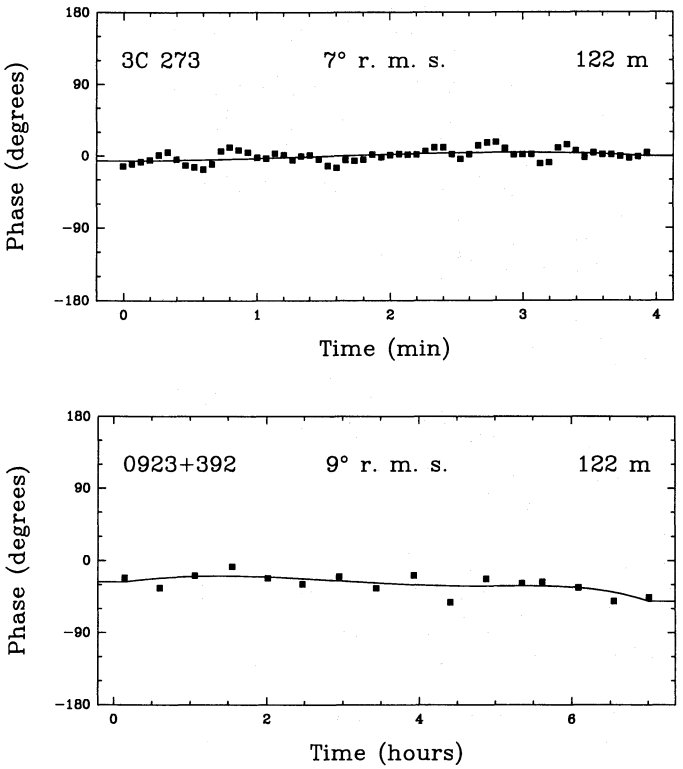

Fig. 7. Short and long term atmospheric phase fluctuations on a 122 m baseline. **a** Phase variations at 115 GHz of 3C 273 (30 Jy) over a 4 min interval (4 s samples). **b** Phase variations at 110 GHz of 0923+392 (3.6 Jy) over several hours (4 min samples).

frequency. Short and long term atmospheric phase fluctuations depend on the water vapor content and baseline length. While σ_p can be up to 60° on the longest baseline under mediocre conditions (7 mm water vapor), 15° is more typical for short (< 100 m) baselines in good conditions (Fig. 7; see also Olmi & Downes 1992).

For these typical values $\delta S = 1.7$–2.8 mJy in a one hour DSB integration at 90 GHz. For a full synthesis with 36 h integration on source, this goes down to about 0.4 mJy. At 115 GHz, the noise is about two times worse because of higher system noise and increased oscillator jitter and atmospheric phase fluctuations.

In a synthesized map the r. m. s. brightness temperature fluctuations are

$$\delta T_b = \frac{\rho\lambda^2}{\theta_1\theta_2}\delta S \approx \frac{\theta_b^2}{\theta_1\theta_2}\frac{T_{sys}}{\eta_c\eta_p\eta_j\sqrt{N(N-1)}\sqrt{\Delta\nu\,\tau}}, \quad (3)$$

where λ is the wavelength, θ_1 and θ_2 are the major and minor beam diameters, the antenna beam diameter $\theta_b = 55''$ at 90 GHz, and $\rho \simeq 15\,\mathrm{K\,Jy^{-1}\,mm^{-2}\,arcsec^2}$ for untapered maps with natural weighting. Tapering increases ρ, but also increases the synthesized beam size.

A spectral map with 625 kHz channel spacing and 36 h integration on source will then have an r. m. s. noise $\delta T_b = 0.14$ K for the CD configurations (3.5″ × 4.1″ beam) or 0.4 K for the BC configurations (2.1″ × 2.3″ beam).

4. Example results

During the astronomical test and commissioning period we carried out several observing programs to refine operations and characterize the interferometer's performance. The results we highlight here illustrate the interferometer's capabilities, most notably the benefits of its high sensitivity.

High resolution spectral line mapping is the principal application of the IRAM interferometer. For example, even though the observations were made during the summer, our HCN(1→0) map of the nearby galaxy IC 342 (Fig. 8; Downes et al. 1992) has nearly the same resolution (2.7″) and one fifth the noise level of the CO(1→0) map (Ishizuki et al. 1990) made with the array at Nobeyama, Japan.

The dynamic range of a map can be dramatically improved by self-calibration techniques. For a map of the HCN(1→0) emission from the molecular outflow in the proto-planetary nebula CRL 618, we used the unresolved continuum source at the center as a phase reference. The resulting dynamic range is 50:1. (Fig. 9; Neri et al. 1992)

Rather than mapping a single source, another way to use the interferometer is to make short observations (snapshots) of a large number of sources, but with limited *uv* coverage for each. Although detailed maps of the sources cannot be constructed, the angular extent of many sources can be rapidly surveyed. For example, a survey of thermal SiO(2→1) emission from circumstellar envelopes (Fig. 10; Lucas et al. 1992) shows the grain formation region is larger than previously expected.

A rather special experiment was mapping the SiO(2→1) masers in Ori A (IRC 2). The relative positions of the maser components have a positional accuracy better than 0.005″, even in the center of the double peaked line profile (Fig. 11). Accurate calibration of the bandpass response enabled us to achieve an

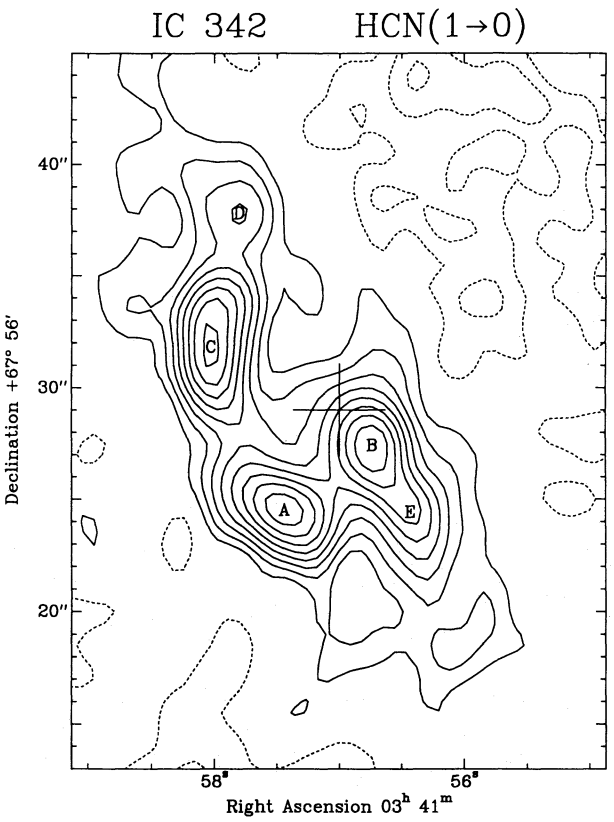

Fig. 8. HCN(1→0) emission from the center of IC 342 integrated over $-15 \leq v_{lsr} \leq 85$ km s^{-1}. The beam diameter is 2.7″ and the contour interval is 10.3 K km s^{-1}, or 5 mJy beam^{-1} (dashed contours negative, zero contour omitted). The cross marks the map's phase center at $03^h41^m57.0^s$, +67°56′29″ (1950) (Downes et al. 1992)

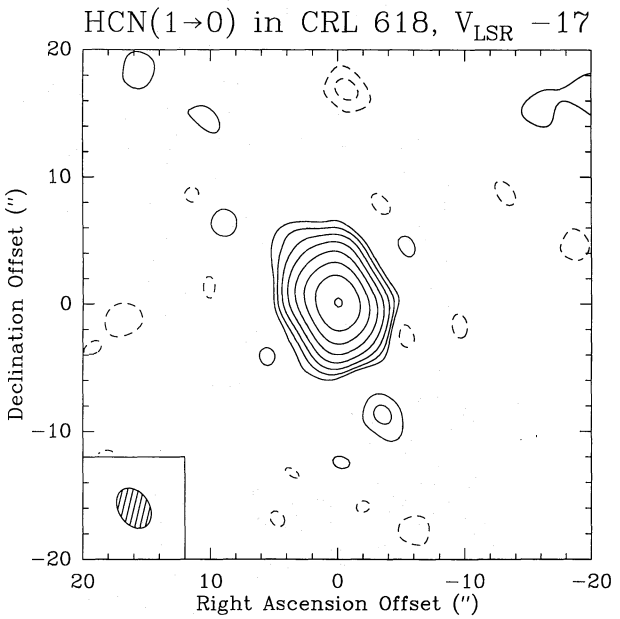

Fig. 9. High dynamic range image of HCN(1→0) emission from the proto-planetary nebula CRL 618 at an LSR velocity of −17 km s^{-1} (Neri et al. 1992). The unresolved 1 Jy continuum source at the center was used as a phase reference and then subtracted from the HCN image. Contour levels are −0.04, −0.02, 0.02, 0.04, 0.08, 0.16, 0.32, 0.64, 1.28, and 2.56 Jy beam^{-1} (dashed contours negative). The insert shows the 2.4″ × 3.4″ beam (FWHM) and the velocity resolution is 3 km s^{-1}.

accuracy three times better than previous measurements (Plambeck et al. 1990) made with the interferometer at Hat Creek, California.

5. Future extensions

Improvements now underway will alleviate some current limitations of the instrument: the maximum contiguous bandwidth covered by the spectral correlator is only 80 MHz, the imaging speed is slow because there are only three antennas, the baseline lengths are < 300 m, and only the 3 mm band can presently be observed.

To accomodate additional antennas and provide more flexible coverage of the IF band, a new correlator will be installed in mid 1992. This is a recirculating design with six independent units tunable anywhere in the IF_2 band. Based on an image rejection mixer with better than 30 dB sideband separation, each unit has two adjacent subbands that together provide 64, 128, or 256 complex channels in a bandwidth adjustable of 20-160 MHz. The spectral resolution is, therefore, adjustable from 78.125 kHz to 2.5 MHz. For continuum measurements, all six units can be operated in parallel to cover 960 MHz. The multiplier boards, based on the NFRA correlator chip (Bos 1989), achieve 88% efficiency with four level sampling. Digital delays are used. Data acquisition and correlator control are done by a Motorola 68030 microprocessor connected to the central computer by Ethernet.

Also in 1992, the Schottky receiver will be replaced by another SIS receiver. A fourth antenna now under construction will be completed in 1993 and will double the number of simultaneous baselines and hence the imaging speed. By 1994 the tracks will be extended by 50% and three new stations added (N30, W20, and W30).

Observations in the 1.3 mm window offer higher spatial resolution, better sensitivity for studies of dust emission, and spectroscopy of the CO(2→1) and other high excitation lines. New four channel receivers to be installed by 1994 will have closed-cycle cryostats with two 80-115 GHz and two 205-270 GHz SIS mixers that are independantly tunable. Simultaneous observations will be possible with any pair of mixers and by switching quickly between the mixers, pointing observations will be made at 3 mm during observations at 1.3 mm.

6. Conclusion

The original design for the IRAM interferometer has been completed and the instrument has an ongoing observational program. Since the first call for guest proposals in October, 1990, more than twenty five projects have been accepted and observed. Observing proposals are reviewed three times per year and should be addressed to the IRAM Scientific Secretariat.

Acknowledgements. The IRAM interferometer is the result of the collective efforts of our many colleagues. The instrument grew out of a proposal by E.-J. Blum and J. Lequeux in the 1970s. E.-J. Blum then contributed substantially to development of the IRAM receiver laboratory. M. J. deJonge energetically directed the institute and construction of the observatory on Plateau de Bure. Until his untimely death in 1986, L. N. Weliachew was the

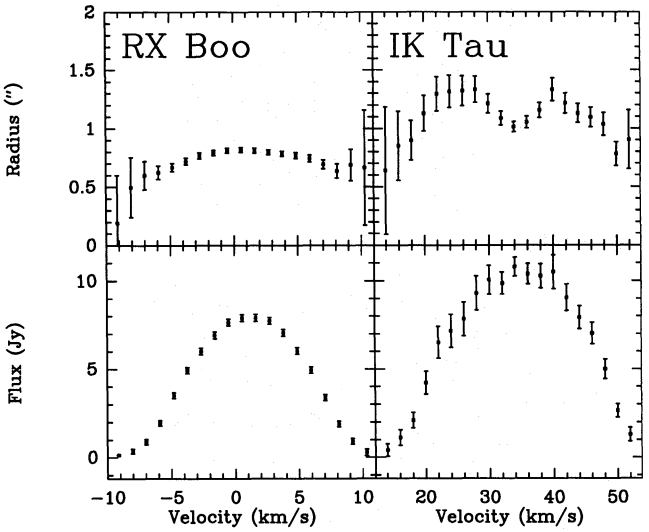

Fig. 10. SiO(2→1) fluxes and half power radii of two circumstellar envelopes as functions of LSR velocity. From a survey of eleven stars (Lucas et al. 1992).

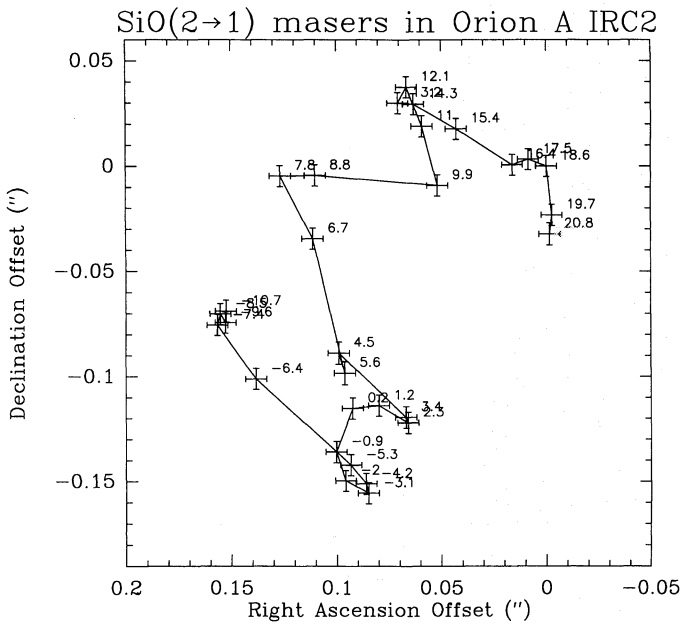

Fig. 11. Relative positions of SiO(2→1) masers in Ori A (IRC 2) labelled by LSR velocity. The 1σ error bars include bandpass calibration errors.

project scientist. Fabrication of the telescope mounts was carried out by Neyrtec (Grenoble, France) and MAN Neue Technologie (Munich, Germany) made the mirrors and backstructures. K. H. Gundlach, J.-L. Pollet, P. Raffin, and M. Vivekanand all contributed substantially to the development and testing of the interferometer. I. Cervera, P. Chaudet, M. Dan, A. Grosz, S. Léonardon, F. Morel, A. Oberti, A. Rambaud, D. Robert, and B. Rossini ensured smooth operation and (when needed) speedy repairs. A. Baudry, R. Bachiller, R. Güsten and C. Henkel helped test and commission the interferometer.

References

Booth, R. S., Delgado, G., Hagström, M., Johansson, L. E. B., Murphy, D. C., Olberg, M., Whyborn, N. D., Greve, A., Hansson, B., Lindström, C. O., & Rydberg, A. 1989, A&A 216, 315
Bos, A. 1986, The NFRA Correlator Chip (NFRA-ITR-176: Dwingeloo)
Castets, A., et al. 1988, A&A 194, 340
Delannoy, J. 1985, in (Sub)Millimeter Astronomy, ed. P. A. Shaver & K. Kjär (ESO: Garching) p25
Delannoy, J. 1991, in Radio Interferometry: Theory, Techniques, and Applications, ed. T. J. Cornwell & R. A. Perley, (ASP, San Francisco) p15
Downes, D. 1989, in Evolution of Galaxies Astronomical Observations, ed. I. Appenzeller, H. Habing, & P. Léna (Springer Verlag: Berlin) p351
Downes, D., Radford, S. J. E., Guilloteau, S., Guélin, M., Greve, A., & Morris, D. 1992, A&A 262, 424
Greve, A. 1978, Infrared Phys. 18, 127
Greve, A., Dan, M., & Peñalver, J. 1992, IEEE Trans. Ant. Prop., in press
Heintz, P., & Emerson, D. T. 1985, in International Symposium on Millimeter and Submillimeter Wave Radioastronomy, ed. J. Gomez-Gonzalez (URSI; IRAM: Granada) p183
Ishizuki, S., Kawabe, R., Ishiguro, M., Okumura, S.K., Morita, K.I., Chikada, Y., & Kasuga, T. 1990, Nature 344, 224
Guilloteau, S. 1990, OBS User's Guide (IRAM: Grenoble)
Guilloteau, S., & Forveille, T. 1989, Grenoble Image and Data Analysis System (GILDAS; IRAM: Grenoble)
Lehnert, T., Grassl, C., Gundlach, K. H., & Blondel, J. 1991, Supercond. Sci. Technol., 4, 419
Lucas, R. 1992, Continuum and Line Interferometer Calibration (CLIC; IRAM: Grenoble)
Lucas, R., Bujarrabal, V., Guilloteau, S., Bachiller, R., Baudry, A., Cernicharo, J., Delannoy, J., Forveille, T., Guélin, M., & Radford, S.J.E. 1992, A&A 262, 491
Olmi, L., & Downes, D. 1992, A&A 262, 634
Neri, R., Garcia-Burillo, S., Guélin, M., Cernicharo, J., Guilloteau, S., & Lucas, R. 1992, A&A 262, 544
Plambeck, R. L., Wright, M. C. H., & Carlstrom, J. E. 1990, ApJ 348, L65
Thompson, A. R., Moran, J. M., & Swenson, G. W., Jr. 1986, Interferometry and Synthesis in Radio Astronomy (Wiley: New York)
Urry, W. L., Thornton, D. D., & Hudson, J. A. 1985, PASP 87, 745

This article was processed by the author using Springer-Verlag LaTeX A&A style file 1990.